Whole-rock major and trace element geochemistry: Alteration Impact

The total major element concentrations of some samples from Yanıklı range from 96.9 wt.% to 98.3 wt.% (ESM 13 Table 1). Two samples, SS-9 and Y-75, from the polymictic phreatomagmatic breccia (CVc-3) were analyzed by PANalytical Omnian V37 quantitive module to determine additional elements in the altered and mineralized zones. The analyses yielded high Ba (0.23-0.32 wt.%), Pb (0.61-0.70 wt.%), Zn (0.55-1.33 wt.%), and S (0.52-0.59 wt.%) concentrations (ESM 13 Table 2), and explain the low total elementary concentrations of some samples. The total major element concentrations of samples from the Hod Maden VMS system range from 100.0 wt.% to 101.6 wt.%, regional volcanic rocks from 100.4 wt.% to 101.3 wt.%, and regional intrusive rocks from 98.9 wt.% to 102.0 wt.% (ESM 13 Tables 3-4).

The loss-on-ignition (LOI) of most samples from Yanıklı ranges from 2.88 wt.% to 12.83 wt.% for the mafic series and 0.83 wt.% to 6.89 wt.% for the felsic series (ESM 13 Table 1; ESM 14 Fig 1-2). Similarly, Hod Maden samples have high LOI values, with the mafic series ranging from 2.47 wt.% to 6.28 wt.% (up to 37.4 wt.%) and the felsic series ranging from 2.15 wt.% to 11.71 wt.% (ESM 13 Table 3; ESM 14 Fig. 1-2). The regional volcanic and intrusive rock samples have low LOI values < 2.7 wt.%, except for one intrusive rock at 4.08 wt.% (ESM 13 Table 4; ESM 14 Fig. 1-2). Therefore, to assess the impact of hydrothermal alteration on element mobility and before rock classification based on whole-rock geochemistry, Harker correlation diagrams were employed to test element mobility or immobility.

The concentrations of TiO_2 and Al_2O_3 in both mafic and felsic rock series is uncorrelated with LOI, except for one felsic samples from Hod Maden, which has the highest LOI and TiO_2 concentrations (ESM 14 Fig. 1). SiO_2 concentration decreases with increasing LOI in both the felsic and mafic series at Yanıklı, and this trend is more pronounced at Hod Maden (ESM 14 Fig.1). The CaO concentrations in most felsic rocks are uncorrelated with LOI, except for a feldspar porphyry dacite (CDa) sample from Yanıklı. In contrast, mafic rocks show a rough positive, though scattered, correlation between higher CaO concentrations and LOI in the Yanıklı samples, indicating variable carbonate alteration (ESM 14 Fig. 1). K_2O concentrations decrease with increasing LOI in the feldspar-phyric flow-banded rhyolite/rhyodacite (CRDa-2) sample from Yanıklı and in the felsic phases of Hod Maden but are scattered in the fine-grained to feldspar-phyric flow-banded and columnar rhyodacite/dacite (CRDa-1) samples from Yanıklı. The mafic series rocks show no correlation between K_2O concentrations and LOI (ESM 14 Fig. 1). Na_2O concentrations are scattered in the felsic series but display a rough negative correlation in the mafic series (ESM 14 Fig. 1). MgO concentrations exhibit a positive correlation with increasing LOI in the felsic series, while no correlation is observed in the mafic series (ESM 14 Fig .1). No significant correlation pattern is observed in the P_2O_5 vs. LOI diagram, with the mafic rocks showing a higher data scatter (ESM 14 Fig. 1).

Zr is considered immobile with respect to increasing LOI, and no prominent correlation is observed in either the felsic or mafic series from both Yanıklı and Hod Maden (ESM 14 Fig. 2). Therefore, we further constrained element mobility using SiO_2, TiO_2, Y, Yb, La, Nb, Dy, and Ta vs. Zr Harker diagrams (ESM 14 Fig. 3).

The positive correlation between SiO_2 and Zr in mafic to felsic rock samples reflects fractional crystallization without zircon removal up to SiO_2 concentrations of approximately 65 wt.% (ESM 14 Fig. 3A; Buchanan et al. 2002; Günther et al. 2018). However, Yanıklı samples from the fine-grained to feldspar-phyric flow-banded and columnar rhyodacite/dacite (CRDa-1) and feldspar-phyric flow-banded rhyolite/rhyodacite (CRDa-2) with SiO_2 concentrations exceeding 65 wt.% show a negative correlation between Zr and SiO_2 (ESM 14 Fig. 3A), indicating progressive zircon fractionation (e.g., Gudelius et al. 2020). The TiO_2 vs. Zr diagram clearly distinguishes the felsic and mafic phases in both Yanıklı and Hod Maden samples. One felsic sample from Hod Maden (EB158) plots in the intermediate phase and exhibits the highest LOI, likely due to alteration. The concentrations of Y, Yb, La, Nb, Dy, and Ta in both the felsic and mafic series are positively correlated with Zr (ESM 14 Fig. 3C-H). These strong trace element vs. Zr correlations suggest that these elements remained largely immobile during hydrothermal alteration in both Yanıklı and Hod Maden. However, one sample (Y-34) from the feldspar porphyry dacite (CDa) shows significant enrichment in Y, Yb, Sm, and Dy, indicating potential hydrothermal alteration effects, like sample EB158 from Hod Maden (ESM 14 Fig. 3C-H).

References

Buchanan P, Reimold W, Koeberl C, Kruger F (2002) Geochemistry of intermediate to siliceous volcanic rocks of the Rooiberg Group, Bushveld Magmatic Province, South Africa. Contrib Mineral Petrol 144:131-143

Gudelius D, Zeh A, Wilson AH (2020) Zircon formation in mafic and felsic rocks of the Bushveld Complex, South Africa: Constraints from composition, zoning, Th/U ratios, morphology, and modelling. Chem Geol 546:119647

Günther T, Haase KM, Klemd R, Teschner C (2018) Mantle sources and magma evolution of the Rooiberg lavas, Bushveld Large Igneous Province, South Africa. Contrib Mineral Petro 173:1953

Legend of the diagrams

Yanıklı

- Fine-grained to feldspar-phyric flow- banded and columnar rhyodacite/dacite (CRDa-1)
- Feldspar-phyric flow-banded rhyolite/rhyodacite (CRDa-2)
- Feldspar-phyric dacite (CDa)
- Very fine-grained andesite (CAn-4)
- Medium- to coarse-grained feldspar-phyric variolitic basalt/basaltic andesite (CAn-3)
- Megacrystic feldspar-phyric andesite (CAn-2)
- Medium- to coarse-grained feldspar-phyric basaltic andesite (CAn-1)

- Hod Maden columnar rhyodacite/dacite
- Kızılkaya Formation rhyodacite/dacite
- Tirebolu Formation rhyolite/rhyodacite
- Hod Maden Çağlayan Formation basaltic andesite
- Çağlayan Formation intermediate volcanic rock
- Hod Maden Çatak Formation basalt

Yanıklı

NE-oriented

- Feldspar-phyric dacitic dike (CDike-1)

NW-oriented

- Feldspar-phyric dacitic dike (CDike-1)
- Feldspar-phyric andesitic to basaltic dike (CDike-2)

ESM 14 Fig. 1

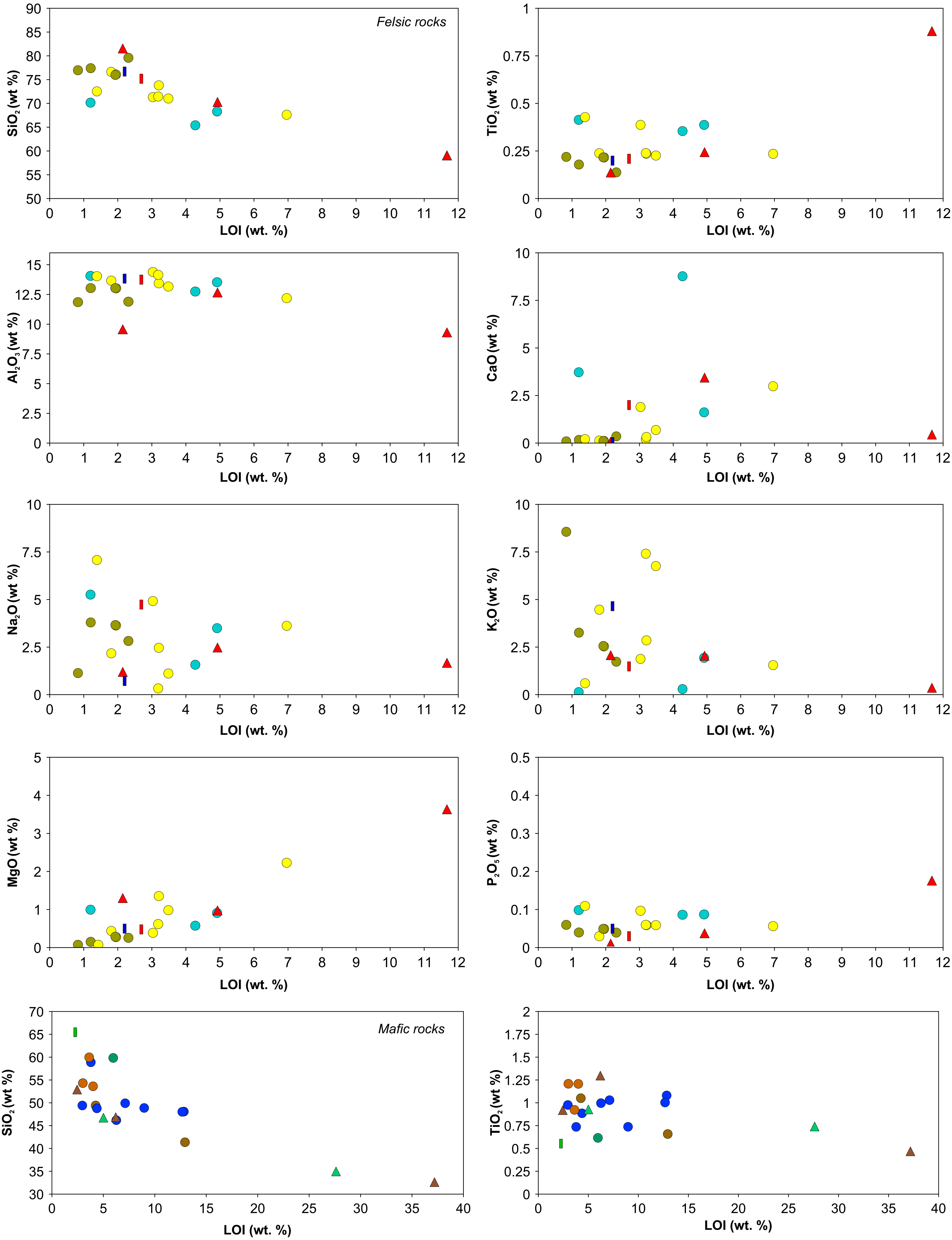
Felsic rocks
SiO_2 (wt %)
TiO_2 (wt %)
Al_2O_3 (wt %)
CaO (wt %)
Na_2O (wt %)
K_2O (wt %)
MgO (wt %)
P_2O_5 (wt %)
Mafic rocks
SiO_2 (wt %)
TiO_2 (wt %)
LOI (wt. %)

ESM 14 Fig. 1 Contd.

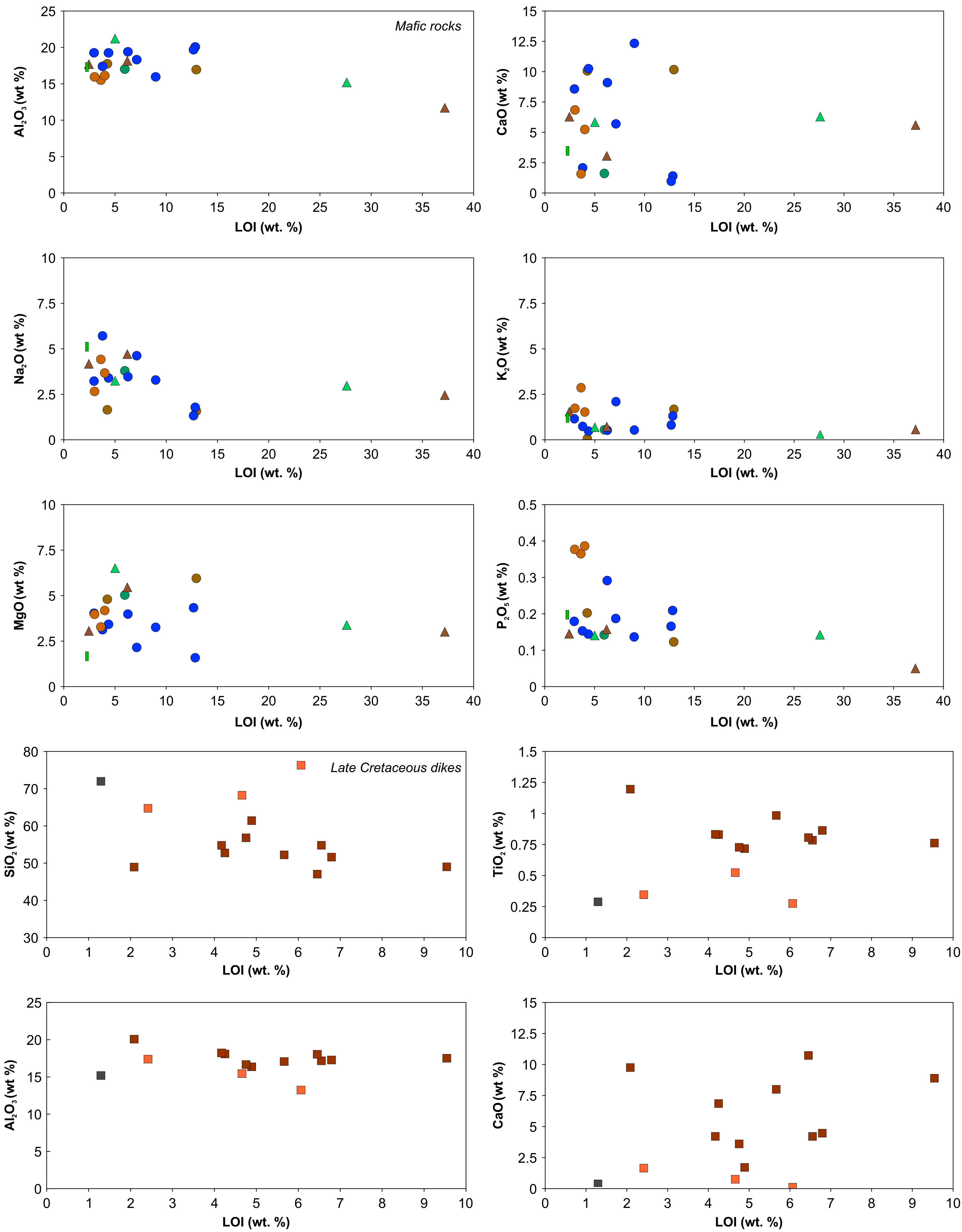

ESM 14 Fig. 1 Contd.

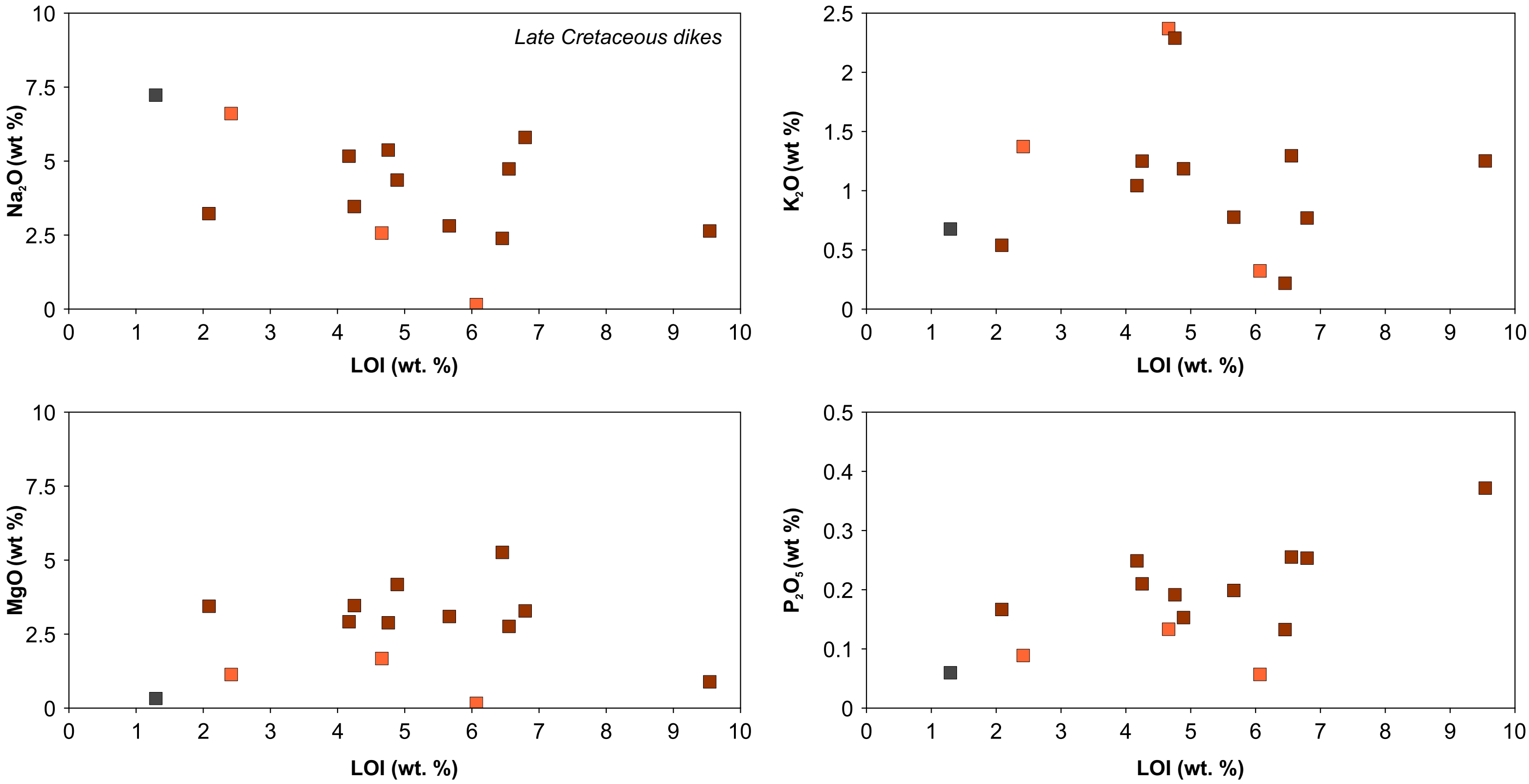

ESM 14 Fig. 2

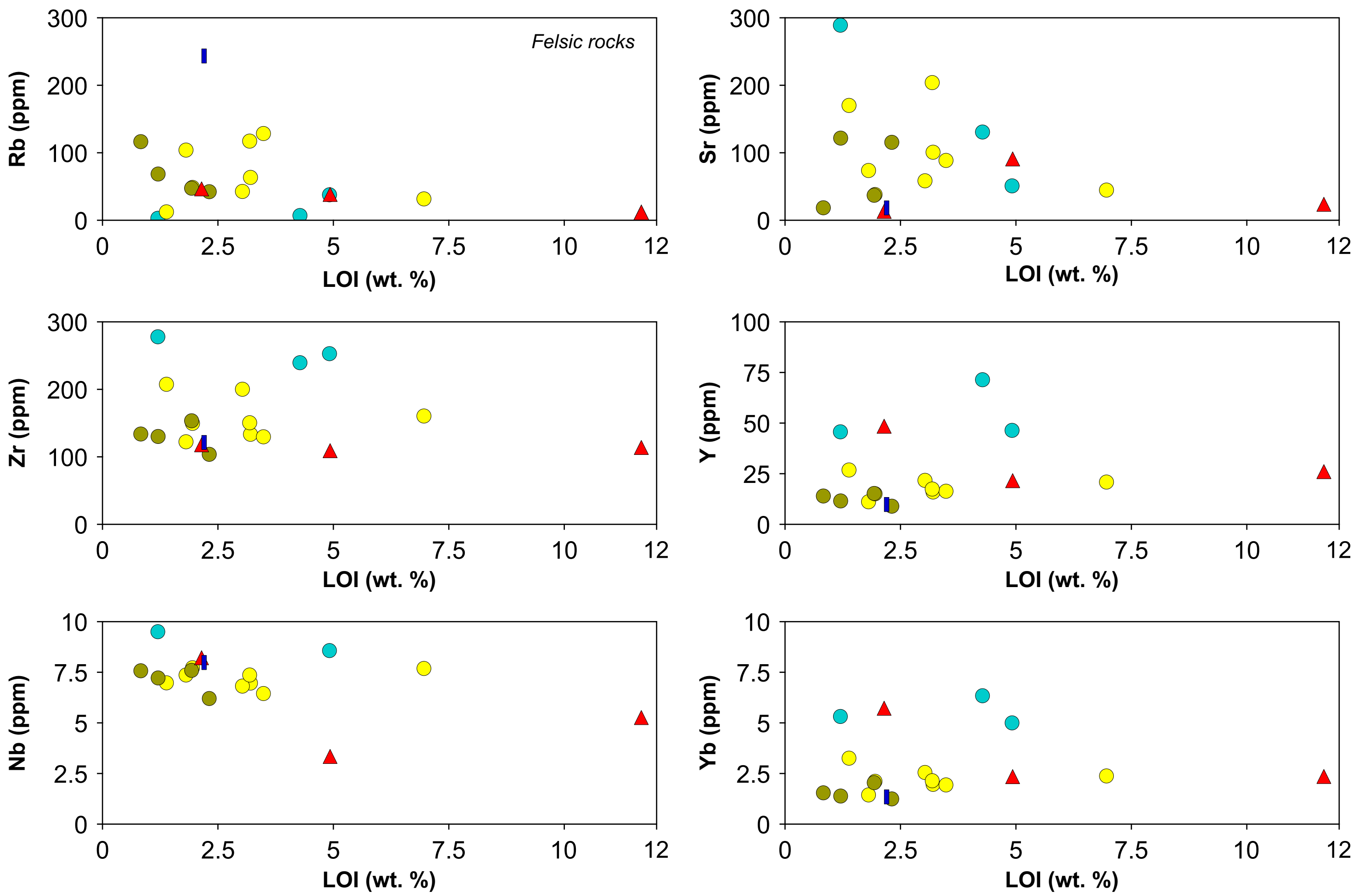

ESM 14 Fig. 2 Contd.

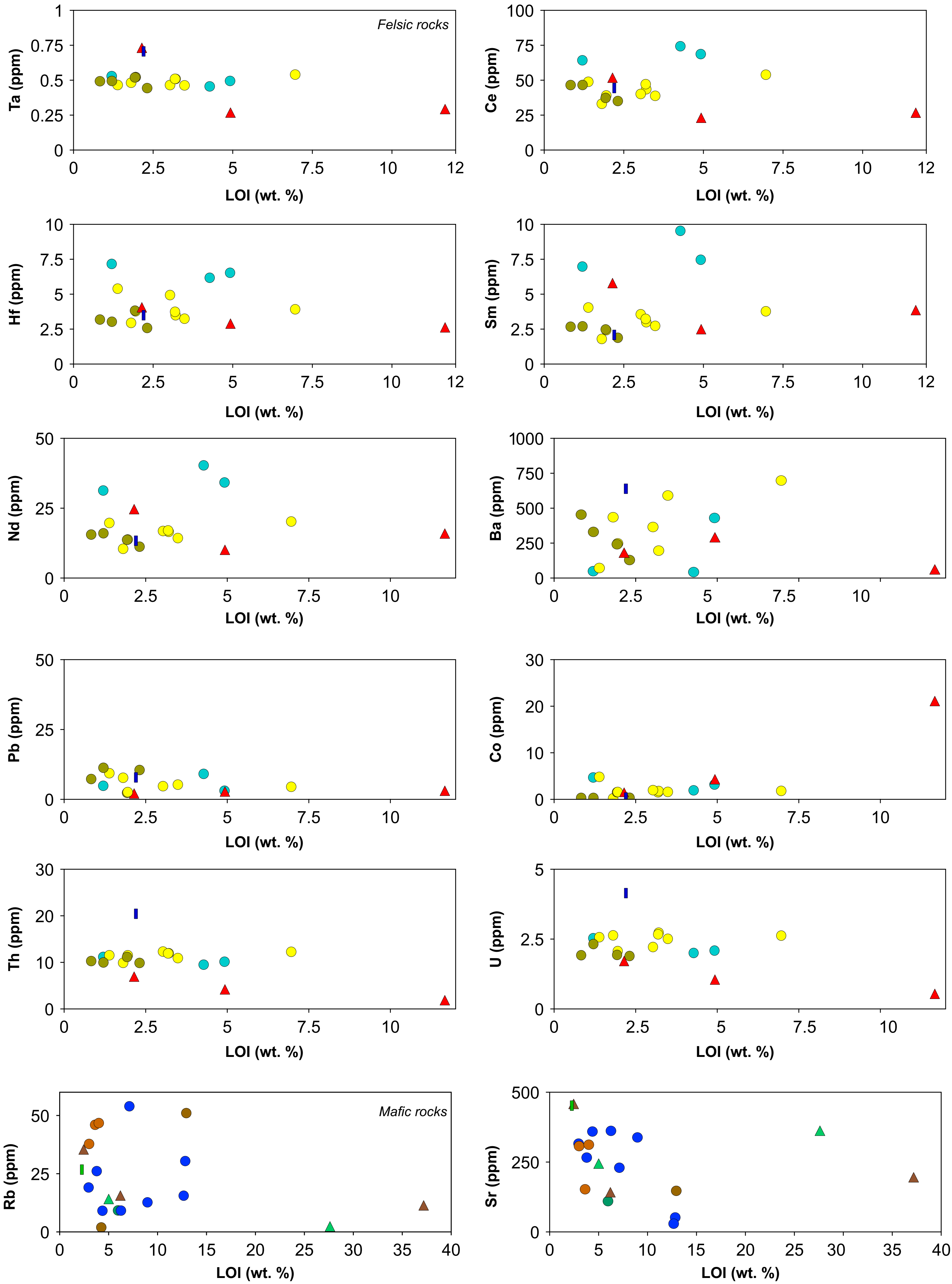

ESM 14 Fig. 2 Contd.

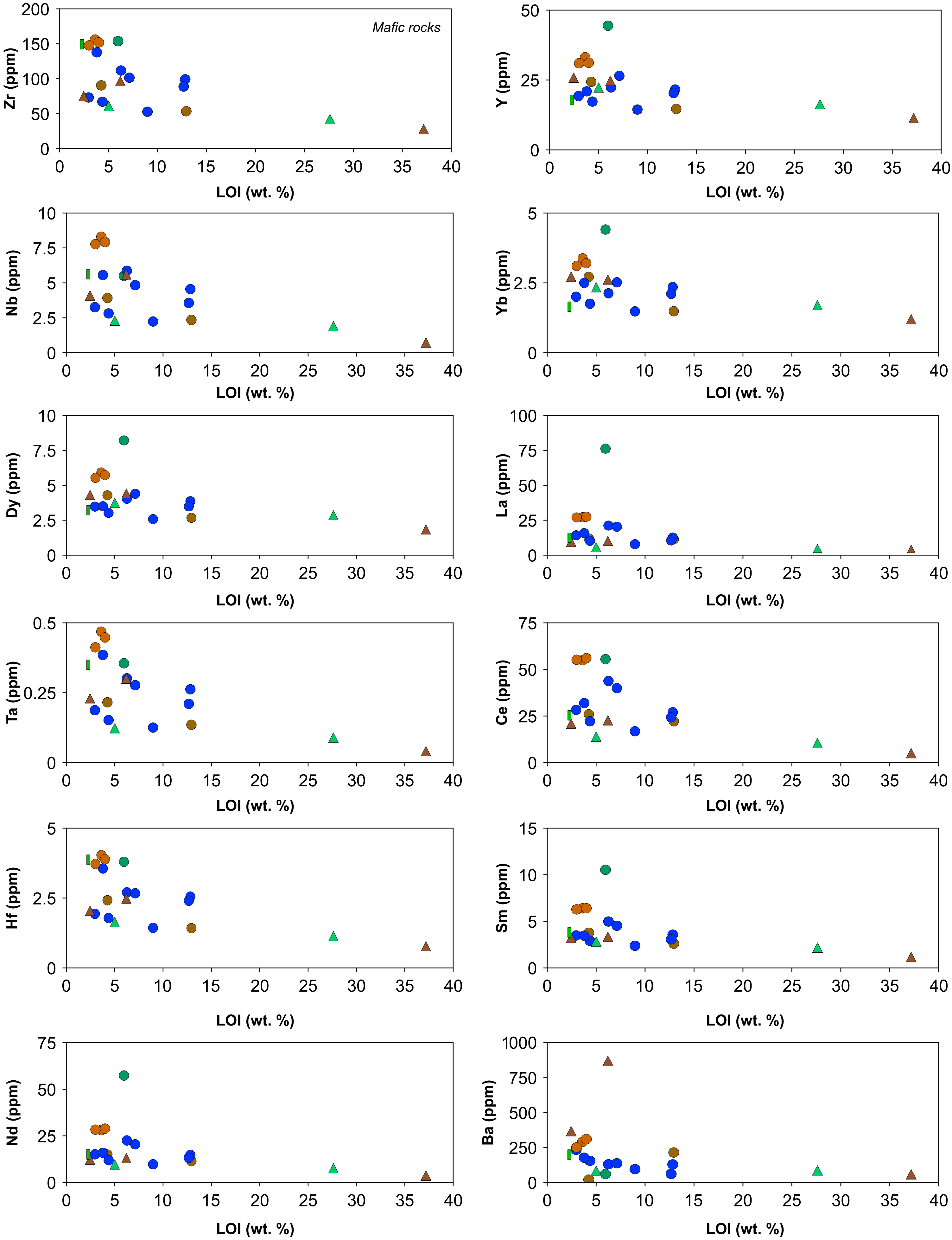

ESM 14 Fig. 2 Contd.

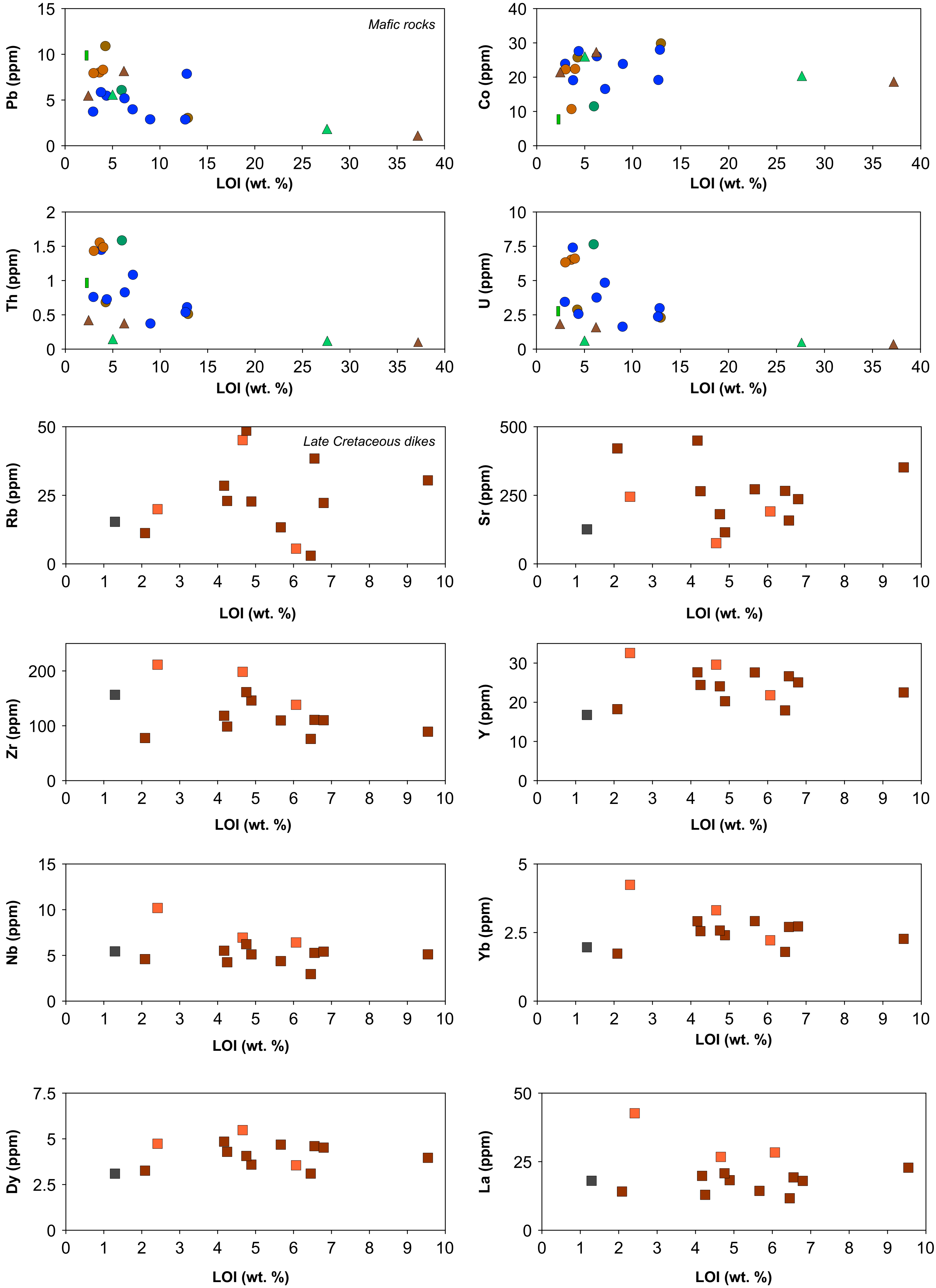

ESM 14 Fig. 2 Contd.

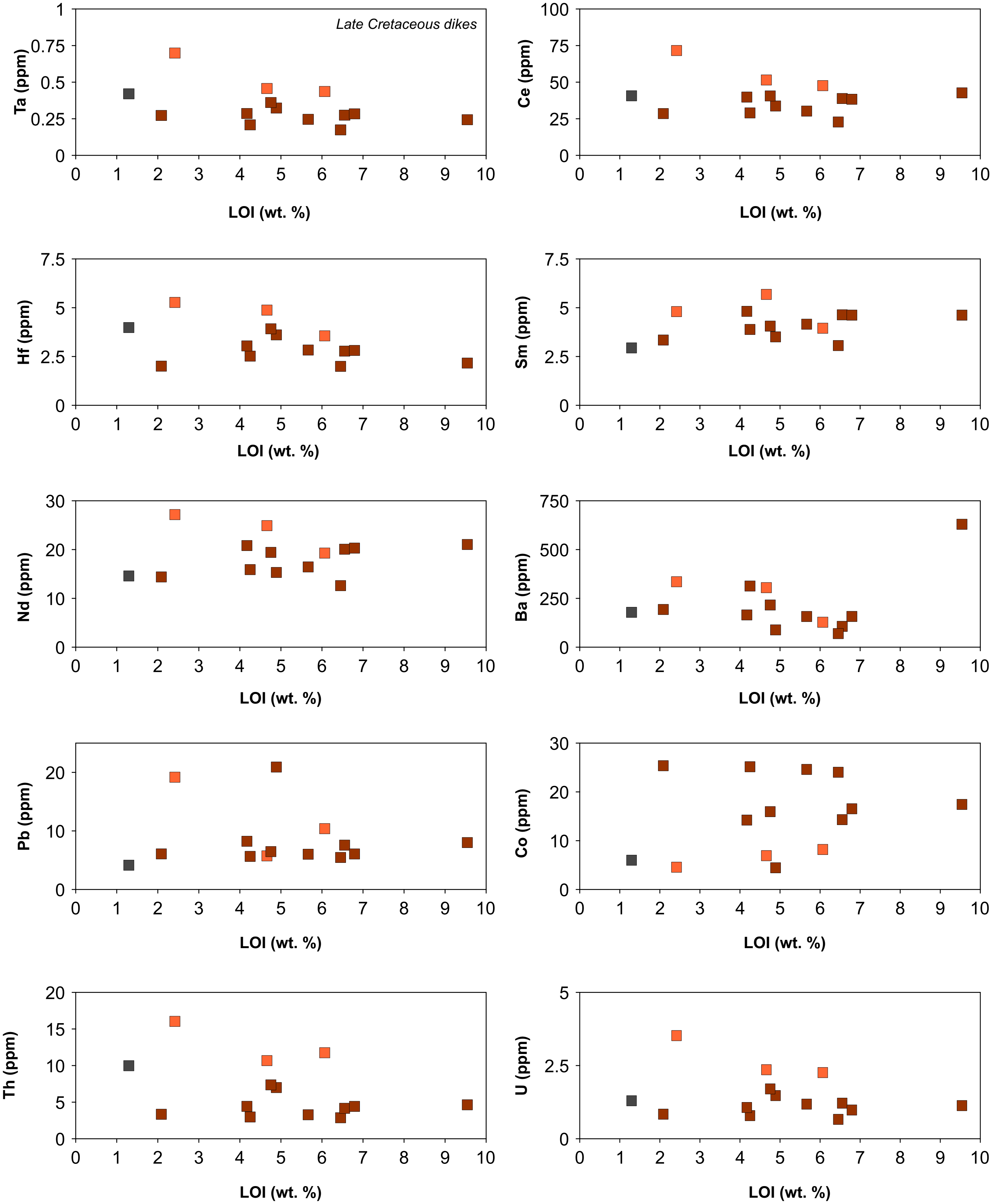

ESM 14 Fig. 3

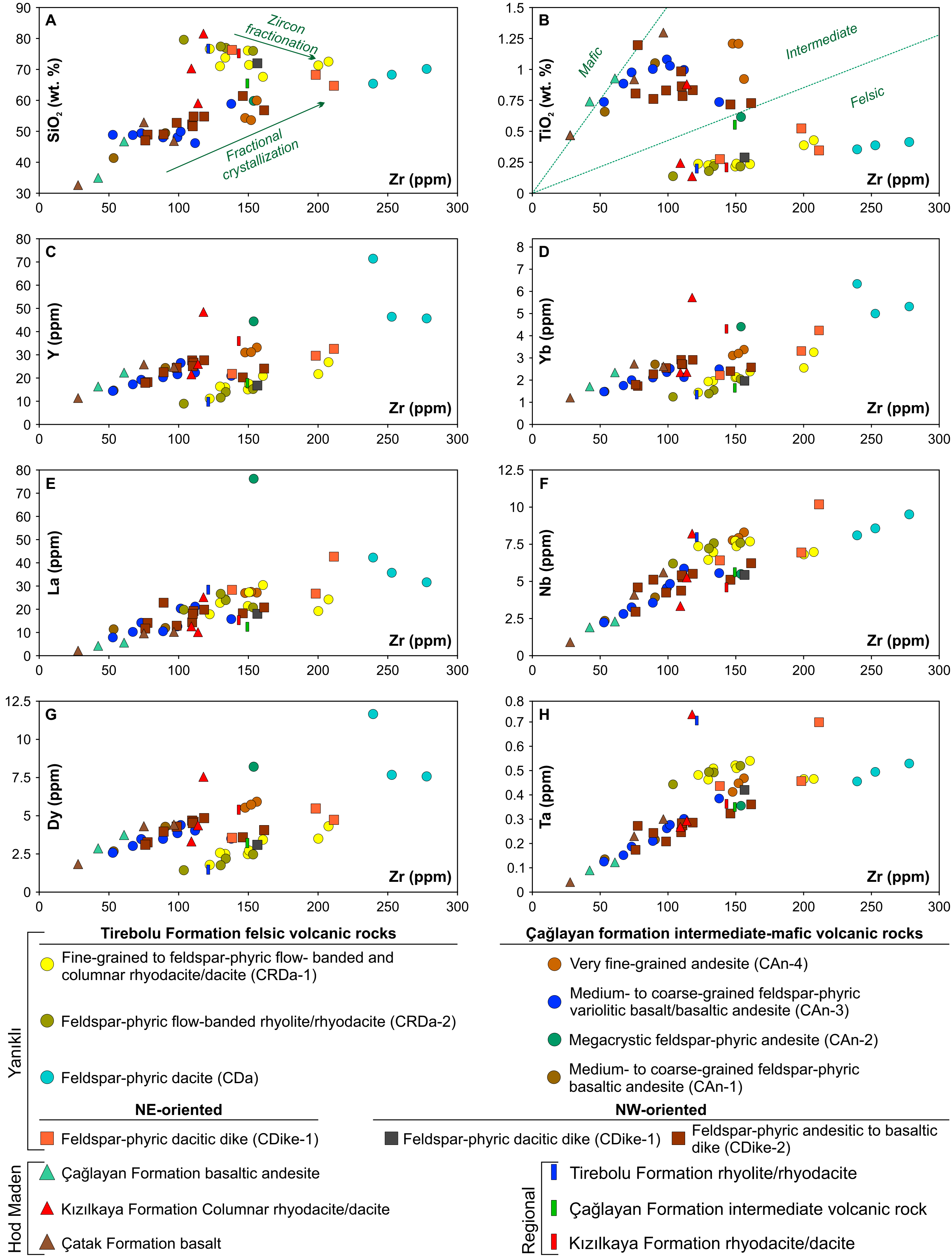

A
SiO2 (wt. %)
Zr (ppm)
Zircon fractionation
Fractional crystallization
B
TiO2 (wt. %)
Zr (ppm)
Mafic
Intermediate
Felsic
C
Y (ppm)
Zr (ppm)
D
Yb (ppm)
Zr (ppm)
E
La (ppm)
Zr (ppm)
F
Nb (ppm)
Zr (ppm)
G
Dy (ppm)
Zr (ppm)
H
Ta (ppm)
Zr (ppm)
Yanıklı
Tirebolu Formation felsic volcanic rocks
Fine-grained to feldspar-phyric flow- banded and columnar rhyodacite/dacite (CRDa-1)
Feldspar-phyric flow-banded rhyolite/rhyodacite (CRDa-2)
Feldspar-phyric dacite (CDa)
Çağlayan formation intermediate-mafic volcanic rocks
Very fine-grained andesite (CAn-4)
Medium- to coarse-grained feldspar-phyric variolitic basalt/basaltic andesite (CAn-3)
Megacrystic feldspar-phyric andesite (CAn-2)
Medium- to coarse-grained feldspar-phyric basaltic andesite (CAn-1)
NE-oriented
Feldspar-phyric dacitic dike (CDike-1)
NW-oriented
Feldspar-phyric dacitic dike (CDike-1)
Feldspar-phyric andesitic to basaltic dike (CDike-2)
Hod Maden
Çağlayan Formation basaltic andesite
Kızılkaya Formation Columnar rhyodacite/dacite
Çatak Formation basalt
Regional
Tirebolu Formation rhyolite/rhyodacite
Çağlayan Formation intermediate volcanic rock
Kızılkaya Formation rhyodacite/dacite